Biexciton Quantum Coherence in a Single Quantum Dot

Gang Chen,[1,*] T. H. Stievater,[1,†] E. T. Batteh,[1] Xiaoqin Li,[1] D. G. Steel,[1] D. Gammon,[2] D. S. Katzer,[2] D. Park,[2] and L. J. Sham[3]

[1]*The FOCUS Center, Harrison M. Randall Laboratory, University of Michigan, Ann Arbor, Michigan 48109*

[2]*The Naval Research Laboratory, Washington, DC 20375*

[3]*Department of Physics, University of California San Diego, La Jolla, California 92093*

(Received 28 August 2001; published 5 March 2002)

Nondegenerate (two-wavelength) two-photon absorption using coherent optical fields is used to show that there are two different quantum mechanical pathways leading to formation of the biexciton in a single quantum dot. Of specific importance to quantum information applications is the resulting coherent dynamics between the ground state and the biexciton from the pathway involving only optically induced exciton/biexciton quantum coherence. The data provide a direct measure of the biexciton decoherence rate which is equivalent to the decoherence of the Bell state in this system, as well as other critical optical parameters.

DOI: 10.1103/PhysRevLett.88.117901 PACS numbers: 03.67.Lx, 03.65.Yz, 78.67.Hc

At the core of quantum information and computation lies the requirement to construct coherent combinations of quantum states [1,2]. The basic quantum operations can be performed on a sequence of pairs of physically distinguishable quantum bits and, therefore, can be illustrated by a simple four-level system shown in Fig. 1. In an optically driven system where the $|01\rangle$ and $|10\rangle$ states can be directly excited, direct excitation of the upper $|11\rangle$ level from the ground state $|00\rangle$ is usually forbidden and the most efficient alternative is coherent nondegenerate two-photon excitation, using $|01\rangle$ or $|10\rangle$ as an intermediate state. However, as is well known in atomic systems (see, for example, [3–5]), excitation of the upper level does not ensure quantum coherence between the upper level and the ground state. Moreover, coherence that is induced can be rapidly lost due to scattering or coupling to other modes (e.g., phonons in solid state systems) leading to a change of the relative phase between the two states without necessarily decaying the individual probability amplitudes (pure dephasing). The loss of probability amplitude and the random change in phase over time cause decoherence of $|\psi\rangle = a|00\rangle + b|11\rangle$ (in the interaction picture), leading to errors in a quantum logic device.

Optically driven semiconductor quantum dots (QD's) have been proposed [6–8] as potential quantum information systems because of their similarities to atomic systems and their key difference in size which gives rise to strongly resonant excitonic transitions and fixed addresses. In the simplest two quantum-bit system within a single QD, the energy level structure in Fig. 1 is given by the ground state (the unexcited dot) as $|00\rangle$, the linearly polarized (i.e., the symmetric and antisymmetric combinations of spin up and down) exciton states as $|01\rangle$ and $|10\rangle$, and the biexciton state of the two antiparallel-spin excitons due to Coulomb coupling as $|11\rangle$.

In this paper, we apply a variant of the resonant coherent nonlinear optical spectroscopy techniques developed in atomic systems [4] to demonstrate the existence of the fully quantum coherent pathway for the formation of the coherent combination of the biexciton state and the ground state $|\psi\rangle = a|00\rangle + b|11\rangle$, and, in the process, measure its decoherence rate. The decoherence of this state is identical to the closely related Bell state with $a = b$. The coherent contribution of the biexciton state is essential for quantum information processing. The contribution of pure dephasing processes of the $|11\rangle$ state relative to the other three states determines the error that accumulates in a quantum operation [8]. Unlike the earlier single dot coherent manipulation experiments which used polarization-controlled excitation to study the exciton dipole coherence [9] and the Zeeman coherence between two single exciton states [10], the biexciton coherence reported here is controlled by two color excitation, a major step forward in terms of the complexities associated with decoherence and in unintended dynamics as shown in [8].

The measurements are performed with two mutually coherent optical fields, $E_1(\Omega_1)$ and $E_2(\Omega_2)$ polarized and tuned, respectively, to excite the $|00\rangle \rightarrow |01\rangle$ and the $|01\rangle \rightarrow |11\rangle$ transitions, as indicated in Fig. 1 (dark arrows). The strong biexciton binding in QD's observed in

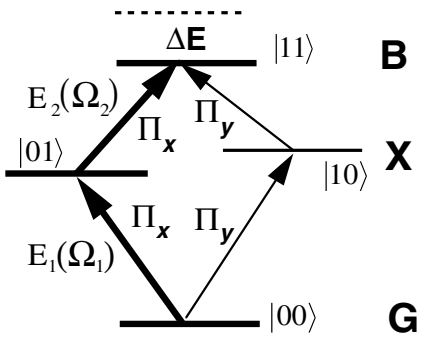

FIG. 1. Model for an elongated single QD. $|11\rangle$, $|01\rangle$ ($|10\rangle$), and $|00\rangle$ denote the biexciton, the exciton, and the ground states, respectively. ΔE is the biexciton binding energy. The optical selection rules for various transitions are indicated.

previous works [11–17] makes the two transitions differentiable in energy using narrow-band fields. The photoluminescence (PL) excitation observation of the two-photon generation of the biexciton in a QD via a virtual intermediate state [11] is an important precursor to the present work on the coherent combination of the biexciton and ground state but the physics of the coherent excitations is distinct from the incoherent transitions between states involved in the PL processes.

In the presence of pure dephasing, optical excitations are most easily described using the density matrix for the optical transitions, $\hat{\rho}$. The excitation of the biexciton state is given by $\rho_{11,11}$. Using the excitation scheme discussed above and in the limit of perturbation theory in the applied fields, the resonant excitation of the biexciton is given by the following typical perturbation sequences [3]:

$$\rho_{00,00} \xrightarrow{E_1(\Omega_1)} \rho_{01,00} \xrightarrow{E_1^*(\Omega_1)} \rho_{01,01} \xrightarrow{E_2(\Omega_2)} \rho_{11,01} \xrightarrow{E_2^*(\Omega_2)} \rho_{11,11}\,,$$

$$\rho_{00,00} \xrightarrow{E_1(\Omega_1)} \rho_{01,00} \xrightarrow{E_2(\Omega_2)} \rho_{11,00} \xrightarrow{E_1^*(\Omega_1)} \rho_{11,01} \xrightarrow{E_2^*(\Omega_2)} \rho_{11,11}\,.$$

The first is referred to as the stepwise excitation pathway and depends on the population (and corresponding decay dynamics) of the exciton. This pathway could be excited even if the optical fields were optically incoherent. The second pathway is the fully coherent two-photon process. Its observation requires the lasers to have a mutual coherence time much greater than the inverse of the decoherence rate of the Bell state.

Data were taken from single GaAs QD's formed by interface disorder in a 42 Å layer of GaAs molecular beam epitaxy grown between 250 Å $Al_{0.3}Ga_{0.7}As$ barriers. High spatial resolution is achieved through an aluminum mask with a series of submicrometer sized apertures. Previous PL studies have revealed sharp resonances from heavy-hole excitons confined to these QD's [18] where elongation along the $[\bar{1}10]$ axis leads to linear polarization selection rules [19].

The biexciton binding energy is denoted by ΔE. We denote the transition frequencies and dephasing rates of the coherences between various states as ω_{ij} and γ_{ij} where, for example, $\omega_{11,01}$ denotes the resonant frequency of the $|01\rangle \rightarrow |11\rangle$ transition, $\gamma_{11,00}$ describes the decay of the two-photon coherence, $\rho_{11,00}$, etc. The state relaxation rate of level $|01\rangle$ is denoted by $\Gamma_{01,00}$. Figure 1 has taken into consideration the QD elongation by noting the collinearly polarized optical selection rules for the $|00\rangle \rightarrow |01\rangle$ or $|10\rangle$ and the subsequent $|01\rangle$ or $|10\rangle \rightarrow |11\rangle$ transitions, as shown in [14,16,19,20] for elongated CdTe and GaAs dots.

The PL spectrum (Π_y polarized) shown in Fig. 2(a) is taken through a $\sim$0.5 μm aperture following excitation in the continuum. The peak intensity at the energy labeled by ε_B shows a quadratic dependence on the excitation intensity below 20 W/cm^2 [inset of Fig. 2(a)] and is attributed to the emission due to the $|11\rangle \rightarrow |01\rangle$ transition of one dot [11,15]. Most of the other lines such as the one at ε_X show a linear dependence on the excitation intensity and are due

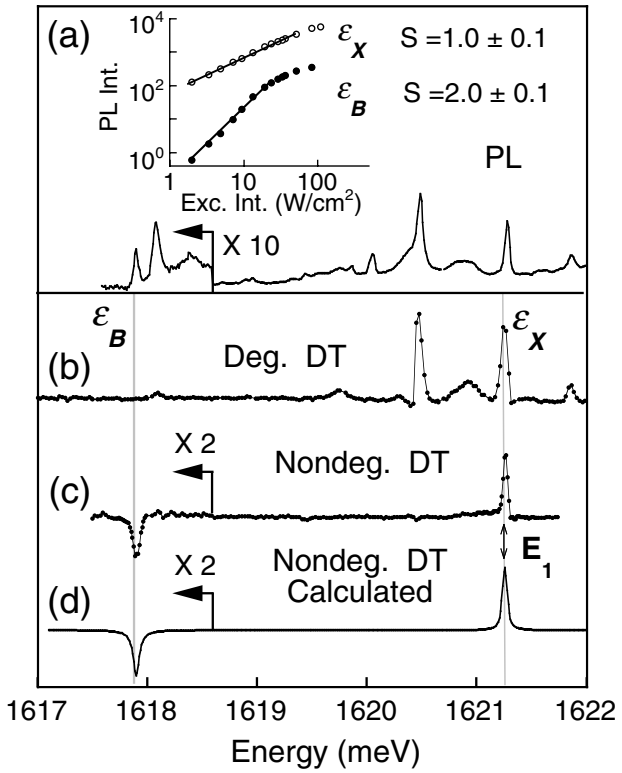

FIG. 2. (a) PL spectrum showing excitonic as well as biexcitonic resonances. The inset shows the integrated PL intensity as a function of the excitation intensity for peaks at ε_X and ε_B. S represents the slope in the log-log scale. (b) Degenerate coherent nonlinear optical spectrum showing only excitonic lines. (c) Spectrum of I_2^{NL}. The spectral dip at ε_B suggests the excitation of biexciton. (d) Theoretical calculation for (c).

to $|01\rangle \rightarrow |00\rangle$ transitions from various dots. From PL, it is not possible to determine if the resonances at ε_B and ε_X are from the same dot. However, we will show below that those two peaks are indeed related.

The two frequency-stabilized CW lasers $E_1(\Omega_1)$ and $E_2(\Omega_2)$ (bandwidth of 4 neV) have a mutual coherence bandwidth of $<$0.1 μeV and are independently tunable. The two fields are amplitude modulated (AM) at two separate modulation frequencies. The stepwise and two-photon paths leading to biexciton formation also lead to third order nonlinear optical polarizations of the form $E_i E_i^* E_j$ $(i \neq j)$. The coherent emission of interest is then selected by homodyne detecting with field E_j^*, and detected at the difference frequency of the two AM modulators [9]. The signal of interest is denoted by I_j^{NL}.

The degenerate response ($\Omega_1 = \Omega_2$) is shown in Fig. 2(b). The data map out the single QD excitonic resonances (such as the ε_X resonance) and are in good agreement with the PL spectrum [9].

I_2^{NL} is shown in Fig. 2(c) as a function of Ω_2 with Ω_1 fixed at the excitonic resonance, ε_X. The strong positive resonance at ε_X corresponds to reduced absorption (saturation) of E_2 caused by E_1 as a result of the excitonic nonlinearity [9]. However, the data show a strong negative spectral feature at ε_B due to the biexciton excitation

arising from both the stepwise and two-photon paths. It corresponds to induced absorption of E_2 leading to formation of the biexciton following the excitation of the exciton by E_1 at ε_X. The transition energies, ε_X and ε_B, agree with those determined in the PL. Their difference yields a ΔE of 3.360 ± 0.001 meV.

In Figs. 2(b) and 2(c), both beams are Π_x polarized, driving the $|00\rangle \rightarrow |01\rangle$ and $|01\rangle \rightarrow |11\rangle$ transitions. Similar results are obtained for Π_y polarization. The negative resonance at ε_B disappears when the two beams are cross-linearly polarized, consistent with the selection rules.

I_2^{NL} can be calculated based on the equations of motion for the model in Fig. 1 following the two quantum mechanical pathways [3,21,22]. We note that both the stepwise and two-photon excitation lead to induced absorption of E_2. The signal is therefore of opposite sign to the excitonic response (saturation). The calculation yields

$$I_2^{\mathrm{NL}} = I_2^{\text{stepwise}} + I_2^{\text{two-photon}} \propto \mathrm{Im}\frac{-i\alpha/\Gamma_{01,00}}{(\gamma_{11,01} + i\Delta_2)}\left(\frac{1}{\gamma_{01,00} + i\Delta_1} + \text{c.c.}\right) + \mathrm{Im}\frac{-i\alpha}{(\gamma_{01,00} + i\Delta_1)(\gamma_{11,01} + i\Delta_2)[\gamma_{11,00} + i(\Delta_1 + \Delta_2)]}, \quad (1)$$

where $\alpha = |\mu_{01,11}\mu_{00,01}E_2E_1|^2$, $\Delta_1 = \Omega_1 - \omega_{01,00}$, and $\Delta_2 = \Omega_2 - \omega_{11,01}$. μ_{ij} is the dipole moment. The spectral dip in Fig. 2(d) is generated as a function of Δ_2 based on Eq. (1) by setting $\Delta_1 = 0$ and is in good agreement with the experiment in Fig. 2(c). The positive peak in Fig. 2(d) is based on calculations for the excitonic response, which is derived in [9].

In the second measurement, we use a variation of the above experiment. Instead of homodyne detecting the nonlinear response with E_2^*, we now homodyne detect the nonlinear response with E_1^* to get I_1^{NL}. In this case, the only perturbation path that contributes to the response is

$$\rho_{00,00} \xrightarrow{E_1(\Omega_1)} \rho_{01,00} \xrightarrow{E_2(\Omega_2)} \rho_{11,00} \xrightarrow{E_2^*(\Omega_2)} \rho_{01,00} \xrightarrow{E_1^*(\Omega_1)} \rho_{01,01}\,.$$

While this path does not lead to the biexciton population, it comes directly from the two-photon coherence $\rho_{11,00}$. It follows that

$$I_1^{\mathrm{NL}} \propto \mathrm{Im}\frac{i\alpha}{(\gamma_{01,00} + i\Delta_1)^2[\gamma_{11,00} + i(\Delta_1 + \Delta_2)]}. \quad (2)$$

Therefore, by detecting E_1, the signal that is due exclusively to a coherent pathway is isolated. In the case that the decoherence of the Bell state is fast ($\gamma_{BG} \gg \Gamma_{XG}$), then I_2^{NL} would be dominated by the stepwise term and I_1^{NL} would be much smaller than I_2^{NL}. The importance of the two-photon coherence can be examined by comparing I_1^{NL} and I_2^{NL}.

The corresponding spectra of I_1^{NL} under various conditions are shown in Figs. 3(a) and 3(b). In 3(a), we show I_1^{NL} as a function of the scanning Ω_2 near ε_B with Ω_1 fixed at ε_X. The response is mainly positive, corresponding to reduced absorption of E_1, in excellent agreement with Eq. (2), as shown by the solid curves. In 3(b), Ω_2 is fixed at ε_B and Ω_1 is tuned around ε_X. The signal comes entirely from the two-photon coherence. The ratio $I_1^{\mathrm{NL}}/I_2^{\mathrm{NL}}$ is measured to be 0.67, showing that the decoherence rate of the biexciton ($\gamma_{11,00}$) is comparable to the exciton energy relaxation rate ($\Gamma_{01,00}$).

From a quantitative analysis, we can extract various decay rates. Specifically, using the line shape in Fig. 3(a) and Eq. (2), we obtain the decoherence rate of the state $|\psi\rangle = a|00\rangle + b|11\rangle$ to be $\gamma_{11,00} = (22.0 \pm 0.7\ \mathrm{ps})^{-1}$, comparable to the excitonic coherence decay rate of $\gamma_{01,00} = (19.5 \pm 4.8\ \mathrm{ps})^{-1}$ and exciton relaxation rate of $\Gamma_{01,00} = (13.3 \pm 5.0\ \mathrm{ps})^{-1}$ obtained by repeating the analysis of [9] on the excitonic feature of Fig. 2. Analysis of the induced absorption line shape in Fig. 2(c) gives $\gamma_{11,01}$ of $(10.5 \pm 1.0\ \mathrm{ps})^{-1}$. Using these decay rates, it is calculated that, with full two-photon coherence contribution, $I_1^{\mathrm{NL}}/I_2^{\mathrm{NL}}$ would be $\sim$0.77, in good agreement with the experimental result above.

Hence, the data show that the pure dephasing of $|00\rangle - |11\rangle$ is insignificant, similar to the single exciton coherence [9], despite the strong exciton-exciton Coulomb interaction. In higher dimensional semiconductor systems and in the absence of disorder, the excitonic and biexcitonic states are characterized by extended Bloch wave functions, which makes them susceptible to purely phase changing interactions with the surrounding crystal, leading to relatively fast dephasing of the two-photon coherence [23]. In QD structures, the 3D confinement results in strong localization which reduces the scattering with continuum excitons and phonons. More importantly, the dephasing rates are independent of the excitation level within the $\chi^{(3)}$ limit, a result profoundly different from higher dimensional systems where the dephasing rate increases with excitation intensity due to exciton-exciton interactions caused by the extended state nature of the wave function [24].

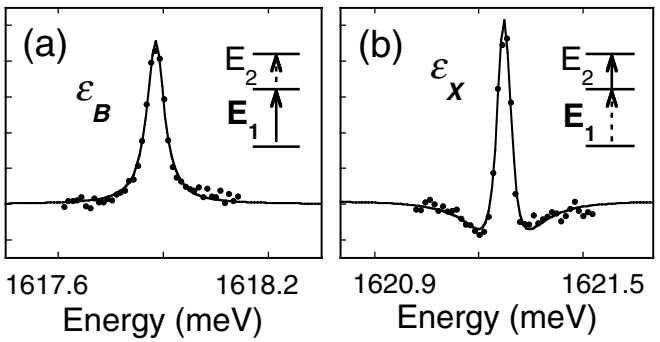

FIG. 3. Spectra of I_1^{NL} (E_1 is detected). (a) E_1 is fixed at ε_X and E_2 is tuned around ε_B. (b) E_2 is fixed at ε_B and E_1 is tuned around ε_X. In the insets, the solid (dashed) arrows denotes the fixed (scanning) fields. Solid curves are the theory.

This work also enables us to study the exciton-biexciton transition dipole moment. Independent measurements based on linear absorption from single quantum dot excitons give a ground state to exciton dipole moment of order 50–100 debye (compared to a few debye for atomic systems) depending on dot size [25]. From the theory above, it is clear that with knowledge of the decay rates and by comparing the signal strength obtained at the biexciton to that obtained at the exciton in Fig. 2(c), it is possible to infer the ratio of the dipole moments. For this particular QD, it is inferred that $\mu_{10,11} \sim \mu_{00,10}$ and hence, the net effect of the Coulomb interaction is not to change the strength of the two transitions, implying that the important interaction effect we exploit is the binding energy.

The above study of the coherence of the biexciton state shows that it can form with the ground state and the two single-exciton states the two-qubit system for quantum information purposes. In general, an antiparallel-spin biexciton state is a linear combination of $|j+, j'-\rangle$, where the indices for each exciton, $j = 1, 2, \ldots$ and $\sigma = \pm$, denote the combination of the jth electron level and the jth hole level excited by σ circularly polarized light. For the excitons excited by the linearly polarized light ($\sigma = x$ or y), the biexciton state $|1x, 1x\rangle$ and $|1y, 1y\rangle$ are the same state as $|1+, 1-\rangle$, because the Pauli exclusion eliminates the double occupancy in $|1\sigma, 1\sigma\rangle$. Hence, both transition paths to the same state in Fig. 1 are then possible. By contrast, the biexciton $|1x, 2x\rangle$ is orthogonal to $|1y, 2y\rangle$ and each state can support only one of these paths. The confinement of the dot isolates the two lowest spin excitons from the other levels and enhances their mutual Coulomb attraction, a conclusion further bolstered by the action of the magnetic field in which the oppositely circularly polarized selection rules for the biexciton are restored.

Finally, as noted above, the state $|\psi\rangle = a|00\rangle + b|11\rangle$ is an entangled state of two excitons. For these measurements, it was necessary to use weak optical fields to maintain the validity of third order nonlinear optical perturbation theory. Hence, the entanglement is far from maximal. However, it has been shown that strong optical pulses can be used to drive the dots into Rabi oscillations [26], thus ensuring that maximally entangled states can be produced.

In summary, this work has demonstrated the coherent two-photon contribution to the resonant optical excitation of the biexciton in a single quantum dot. By exploiting the unique spectral dependences in resonant coherent nonlinear spectroscopy with the power of phase sensitive homodyne detection, we were not only able to demonstrate a direct correspondence between a given exciton and its associated biexciton, we were also able to isolate the part of the wave function induced by the coherent excitation associated with the quantum superposition between the $|00\rangle$ state and the $|11\rangle$ state and measure its decoherence rate. While single particle excitations of individual coupled quantum dots form the basis of scalable quantum computers [6,7] and the system described here is not readily scalable beyond two quantum bits, this system has been proposed as a model two-qubit solid state quantum system for demonstrating a two-qubit quantum-controlled-not-gate and the Deutch-Josza algorithm [8]. The present work, combined with the recent demonstration of Rabi switching in this system [26], indicates that such a demonstration may now be feasible.

This work was supported in part by the National Security Agency, Advanced Research and Development Activity, the Air Force Office of Scientific Research, the National Science Foundation, and DARPA/Spins. D. G. S. thanks the Guggenheim Foundation for support. The authors thank P. Berman, R. Merlin, and M. Scully for discussions.

*Present address: Bell Labs, Lucent Technologies, Murray Hill, NJ 07974.

†Present address: Naval Research Laboratory, Washington, DC 20375.

[1] M. A. Neilson and I. L. Chuang, *Quantum Computation and Quantum Information* (Cambridge University Press, Cambridge, 2000).
[2] C. Macchiavello, G. M. Palma, and A. Zeilinger, *Quantum Computation and Quantum Information Theory* (World Scientific, Singapore, 2000).
[3] I. M. Beterov and V. P. Chebotaev, Prog. Quantum Electron. **3**, 1 (1974).
[4] P. F. Liao, J. E. Bjorkholm, and P. R. Berman, Phys. Rev. A **20**, 1489 (1979).
[5] B. W. Shore, *The Theory of Coherent Atomic Excitation* (Wiley, New York, 1990), Vol. 2.
[6] A. Ekert and R. Jozsa, Rev. Mod. Phys. **68**, 733 (1996).
[7] E. Biolatti *et al.,* Phys. Rev. Lett. **85**, 5647 (2000).
[8] P. Chen, C. Piermarocchi, and L. J. Sham, Phys. Rev. Lett. **87**, 067401 (2001).
[9] N. H. Bonadeo *et al.,* Phys. Rev. Lett. **81**, 2759 (1998).
[10] G. Chen *et al.,* Science **289**, 1906 (2000).
[11] K. Brunner *et al.,* Phys. Rev. Lett. **73**, 1138 (1994).
[12] M. Bayer *et al.,* Phys. Rev. B **58**, 4740 (1998).
[13] G. Bacher *et al.,* Phys. Rev. Lett. **83**, 4417 (1999).
[14] V. D. Kulakovskii *et al.,* Phys. Rev. Lett. **82**, 1780 (1999).
[15] Q. Wu *et al.,* Phys. Rev. B **62**, 13 022 (2000).
[16] L. Besombes, K. Kheng, and D. Martrou, Phys. Rev. Lett. **85**, 425 (2000).
[17] K. Hinzer *et al.,* Phys. Rev. B **63**, 075314 (2001).
[18] D. Gammon *et al.,* Science **273**, 87 (1996).
[19] D. Gammon *et al.,* Phys. Rev. Lett. **76**, 3005 (1996).
[20] K. Bott *et al.,* Phys. Rev. B **48**, 17 418 (1993).
[21] Y. Z. Hu *et al.,* Phys. Rev. Lett. **64**, 1805 (1990).
[22] T. Takagahara, Phys. Rev. B **39**, 10 206 (1989).
[23] K. Ferrio and D. G. Steel, Phys. Rev. B **54**, R5231 (1996).
[24] H. Wang *et al.,* Phys. Rev. Lett. **71**, 1261 (1993).
[25] J. R. Guest *et al.* (to be published).
[26] T. H. Stievater *et al.,* Phys. Rev. Lett. **87**, 133603 (2001).